Palaeogeography, Palaeoclimatology, Palaeoecology 363–364 (2012) 48–56

Contents lists available at SciVerse ScienceDirect

Palaeogeography, Palaeoclimatology, Palaeoecology

journal homepage: www.elsevier.com/locate/palaeo

Late Quaternary productivity changes from offshore Southeastern Australia: A biomarker approach

Raquel A. Lopes dos Santos [a,*], Daniel Wilkins [b,1], Patrick De Deckker [b], Stefan Schouten [a]

[a] NIOZ Royal Netherlands Institute for Sea Research, Department of Marine Organic Biogeochemistry, P.O. Box 59, 1790 AB Den Burg, Texel, The Netherlands
[b] Research School of Earth Sciences, The Australian National University, Canberra, ACT 0200, Australia

ARTICLE INFO

Article history:
Received 27 January 2012
Received in revised form 16 August 2012
Accepted 28 August 2012
Available online 7 September 2012

Keywords:
Primary productivity
Murray Canyons
Diol index
Alkenones
Planktonic foraminifera $\delta^{13}C$
Nutrients

ABSTRACT

Reconstructions of primary productivity at low latitudes have been the focus of several studies to better understand how the export of nutrient-rich, intermediate Southern Ocean (SO) waters influences productivity at these latitudes. This was triggered by the general observation of minima in the planktonic foraminiferal $\delta^{13}C$ values during deglaciations, which was interpreted as an isotopic signal of intermediate SO waters, together with a concomitant increase in diatom productivity at some equatorial sites. However, the impact of these SO waters on productivity at higher latitudes is not well constrained. Here, we compare a high-resolution planktonic foraminiferal $\delta^{13}C$ record with total organic carbon and biomarker records for *Proboscia* diatoms and haptophytes in marine sediments from offshore Southeastern Australia. The planktonic foraminiferal $\delta^{13}C$ record shows distinct minima during deglaciations and the Marine Isotope Stage 4/3 transition, tentatively suggesting that ^{13}C-depleted SO waters reached the coast of Southeastern Australia. However, it did not result in increased productivity during these periods. Instead, the highest primary productivity period, as indicated by total organic carbon and alkenone accumulation rates, occurred during the Last Glacial Maximum while *Proboscia* diatoms mainly proliferated during interglacials and Marine Isotope Stage 3 matching periods of increased diatom productivity in some sites of the Eastern Equatorial Pacific. Our study suggests that increased primary productivity offshore Southeastern Australia was mainly due to stronger westerly winds during glacial periods while *Proboscia* diatom productivity was probably controlled by the transport of silicic acid to this area.

1. Introduction

Understanding the long-term oceanographic controls on primary productivity in lower latitudes of the southern hemisphere has been the aim of numerous studies. In particular, studies have focused on understanding the role of Sub-Antarctic Mode Water (SAMW) and Antarctic Intermediate Water (AAIW) in controlling productivity at lower latitudes (Toggweiler et al., 1991; Brzezinski et al., 2002; Matsumoto et al., 2002; Sarmiento et al., 2004; Crosta et al., 2007; Calvo et al., 2011). This was triggered by the general observation of minima in planktonic foraminiferal $\delta^{13}C$ values during deglaciations, which is commonly interpreted as an isotopic signal of ^{13}C-depleted, CO^2-rich, deep Southern Ocean (SO) waters transported through intermediate water masses such as the SAMW and AAIW (Spero and Lea, 2002; Pena et al., 2008; Calvo et al., 2011; Hayes et al., 2011; Horn et al., 2011). These periods of isotopic minima are contemporaneous with elevated diatom productivity in the Equatorial Pacific (Calvo et al., 2011; Hayes et al., 2011), suggesting that the influx of nutrients, in particular silicic acid, by intermediate waters stimulated diatom productivity at the lower latitudes. However, the impact of these nutrient-rich intermediate waters at higher latitudes is less well constrained.

In the southern hemisphere, most palaeoproductivity studies are focused on equatorial, Antarctic or upwelling regions (Romero et al., 2003; Willmott et al., 2010; Calvo et al., 2011) but few exist from offshore Southeastern Australia (Gingele and De Deckker, 2005). However, offshore Southeastern Australia, and more specifically, the Murray Canyons area probably receives intermediate waters from the SO that originate from the Sub-Antarctic and Antarctic region as discussed by Passlow et al. (1997) from offshore Victoria (37°S, 137°E) to the east of the canyons area, suggesting that this area may be useful to evaluate the impact of SO waters on past productivity. A reconstruction of late Quaternary fluctuations in primary productivity in the Murray Canyons area was previously done by Gingele and De Deckker (2005), relying mainly on sediment records of carbonate content, total organic carbon (TOC) and the stable isotopic composition of planktonic foraminifera. These authors found that increased productivity, inferred from elevated TOC contents, occurred during periods of insolation minima. Gingele and De Deckker (2005) also reported the absence of biogenic silica in sediments, possibly due to dissolution, and therefore could not reconstruct past diatom productivity. Additionally, their $\delta^{13}C$ and TOC

* Corresponding author.
E-mail address: raquel.santos@nioz.nl (R.A. Lopes dos Santos).
[1] Present address: Australian Antarctic Division, Department of Sustainability, Environment, Water, Population and Communities, Kingston, TAS 7050, Australia.

0031-0182/$ – see front matter © 2012 Elsevier B.V. All rights reserved.
http://dx.doi.org/10.1016/j.palaeo.2012.08.013

records were in relatively low resolution for some time periods, making recognition of, for example, minima in $\delta^{13}C$ of planktonic foraminifera difficult.

In the present study, we re-examined the Murray Canyons core MD03-2607 studied by Gingele and De Deckker (2005) and substantially increased the resolution of TOC, $\delta^{13}C$ and $\delta^{18}O$ of planktonic foraminifera records. In addition, we used organic biomarker records for haptophyte algae (alkenones) and relative abundance of *Proboscia* diatoms (Diol index, Rampen et al., 2008) to reconstruct past productivity. Alkenones are established biomarkers to measure past haptophyte algae abundance (e.g. Volkman et al., 1980). The Diol index is the ratio of long chain 1,14 diols produced by *Proboscia* diatoms (Sinninghe Damsté et al., 2003), relative to long chain 1,15 diols (or 1,13 diols) that are produced by eustigmatophytes (Volkman et al., 1992). *Proboscia* diatoms grow in the early stages of upwelling when nutrient concentrations strongly increase (Koning et al., 2001; Smith, 2001). The Diol index has been used to reconstruct variations in past *Proboscia* diatom productivity in the Arabian Sea and in the SO and related to changing nutrient conditions (Rampen et al., 2008; Willmott et al., 2010). We compare our productivity records with the stable carbon isotopic signal in planktonic foraminifera to identify the timing of the advection of water masses from the SO into the Southeastern Australia region and its influence on (past) productivity levels.

2. Core location and regional setting

Piston core MD03-2607 (36°57.64′S; 137°24.39′E) was acquired in the Murray Canyons area at 865 m water depth, east of Sprigg Canyon (Fig. 1). This sediment core was retrieved from a gently sloping plateau, which is separated from the main shelf break by the upper Sprigg Canyon to avoid any significant erosion or deposition of turbidites (Hill and De Deckker, 2004; Gingele and De Deckker, 2005).

The Murray Canyons Group is a vast system of deep-sea canyons located offshore southern Australia that descend to ~5000 m water depth (Hill and De Deckker, 2004) and is influenced by several deep, intermediate and surface water masses. The Circumpolar Deep Water (CPDW), a water mass derived from the Antarctic Circumpolar Current, is the main deep current in the area and is divided into lower CPDW and upper CPDW. Together, the CPDW flows from ~4000 to 1100 m depth (Passlow et al., 1997). Two intermediate water masses were identified around this area: the Antarctic Intermediate Water (AAIW) flowing around 1100–850 m depth and the Sub-Antarctic Mode Water (SAMW) flowing around 850–450 m depth (Passlow et al., 1997). Apart from these water masses, two coastal currents with opposite direction occur in the area: the Leeuwin Current (LC) and its extension (the South Australia Current — SAC), flowing eastward and the Flinders Undercurrent (FC) that flows westward. The LC is a warm surface current that flows southward along the coast of Western Australia, then turns eastward and continues towards the Great Australian Bight. It is strongest in winter, when eastward local winds prevail, but during summer this current weakens and the SAC enhances in the western Great Australian Bight (Middleton and Bye, 2007). The LC is particularly prominent offshore southern Australia during La Niña years (De Deckker et al., 2012). The FC originates from SO waters and has its maximum amplitude at around 600 m depth. It is stronger in summer when the LC is weaker and, together with favourable winds, it can induce weak to moderate coastal upwelling (Middleton and Bye, 2007). This is particularly evident east of the Murray Canyons area along the Bonney coast.

3. Methods

3.1. Chronology and stable isotopic composition of foraminifera

The age model of the upper part of the core was derived from 13 Optically Stimulated Luminescence (OSL) (Table 1) and 22 Accelerator Mass Spectrometry (AMS) radiocarbon (^{14}C) dates (Table 2) measured from the upper 430 cm (~35 ka) of core MD03-2607 (Wilkins, 2009). Following the procedures described in Wilkins et al. (2012),

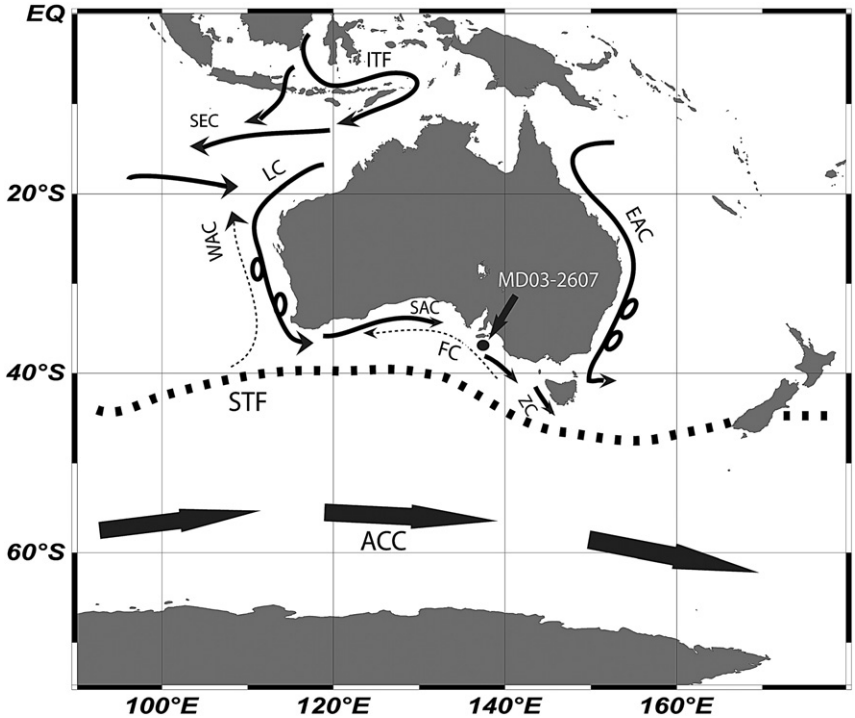

Fig. 1. Location of core MD03-2607 offshore Southeastern Australia (black dot) together with the modern position of the subtropical front (STF — dashed line) and the main currents around Australia (arrows). ITF — Indonesian Troughflow, LC — Leeuwin Current, SAC — South Australia Current, FC — Flinders Undercurrent (dotted arrow means subsurface current), ZC — Zeehan Current, WAC — West Australia Current (dotted arrow means subsurface current), EAC — East Australia Current, SEC — South Equatorial Current, ACC — Antarctic Circumpolar Current. Map was generated with the Ocean Data View software.

OSL dates were measured on single grains or very small aliquots of sand-sized quartz (63–90 μm) loaded into discs containing a 10×10 array of 300 μm wells using the modified single-aliquot regenerative-dose (SAR) protocol of Olley et al. (2004). Lithogenic radionuclide activities were measured by high resolution gamma spectrometry on 7 bulk sediment samples, with 4 of these samples also measured by alpha spectrometry. Dose rates were calculated using the equations of Stokes et al. (2003), iteratively adjusting for the small excess of ^{230}Th and ^{231}Pa until the sample age was stable.

AMS ^{14}C dates were measured on planktonic foraminifera (mixed *Globigerina bulloides* and *Globigerinoides ruber*) from 19 sample depths (Table 2). Results are presented as calibrated ages corrected for the regional marine reservoir using the Marine04 dataset in Calib 5.0.1 (ages <26.0 ka) or the polynomial of Bard (1998) for ages >26.0 ka (Stuiver and Reimer, 1993; Bard, 1998; Reimer and Reimer, 2001; Hughen et al., 2004). Benthic foraminifera (mixed *Cibicidoides mundulus* and *Cibicidoides wuellerstorfi*) were also dated from sediment at 175 cm depth. An additional planktonic sample from the top of a nearby multi-core (MC03) was dated at the AMS facility at the Australian Nuclear Science and Technology Organization to obtain a ^{14}C age from the modern sediment water interface (Fink et al., 2004).

Samples were dissolved in an evacuated glass reaction chamber with supersaturated (105% v/v) phosphoric acid, the resultant gas was cryogenically purified, with CO_2 transferred to glass vessels along with ultra-high-purity H_2 and graphitized overnight at 550 °C with 3–6 mg of iron powder catalyst (Vogel, 1984). The resulting graphite was pressed into a 1 mm central hole in aluminum sample holders and plugged from behind with a short length of aluminum wire as reported by Fifield et al. (1994). The percentage of modern carbon (pMC) of each of the graphite targets was measured with the 14UD Pelletron Tandem Accelerator of the Department of Nuclear Physics at the ANU (Fifield et al., 1994). Uncertainties in pMC values are reported with an additional 2% error added in quadrature to the uncertainty due to counting statistics in order to account for accelerator reproducibility.

The age model of the lower part of the core was based on oxygen isotope stratigraphy of *G. bulloides* tuned to a stacked benthic foraminifer record (Lisiecki and Raymo, 2005). Although the oxygen isotopic stratigraphy of benthic foraminifers is preferred for tuning the age model, as temperature variations are minimal, there were insufficient benthic foraminifera present throughout the core to obtain a continuous record. Previous stable isotope analyses on foraminifera were published in Gingele et al. (2004); however, additional analyses were required in order to improve the age resolutions and the δ^{13}C record, especially for Marine Isotope Stages (MIS) 5 and 6. The sediment core was therefore sampled at 5 cm intervals for foraminiferal tests for the first 200 cm and at ~10 cm interval for the remainder of the core. A minimum of 10 calcite tests, previously cleaned, were softly crushed to open their chambers and to homogenize the material. Samples weighing from 40 to 60 μg were analyzed on a Thermo Finnigan MAT253 with Kiel IV device with a precision of <0.1‰ against the NBS19 standard. All samples were analyzed in duplicate with a maximum value of standard deviation of ~0.4‰. Comparison of the oxygen isotope record of *G. bulloides*, i.e. the combined data from Gingele et al. (2004) and those generated here, with the stacked record of Lisiecki and Raymo (2005) and a benthic foraminifera record from a core east of New Zealand (Elderfield et al., 2010) show a number of similar features which were used as tie points for the age model (Fig. 2). The age model was used to calculate sedimentation rates.

3.2. Total organic carbon measurements

Samples for TOC measurements were taken approximately every 10 cm through most of the core. The sediments were acidified with 2 M HCl overnight to remove carbonate, neutralized using distilled water and freeze dried. TOC was determined using a Flash 2000 organic elemental analyzer with a thermal conductivity detector. Mass accumulation rates of TOC was estimated based on sedimentation rates and assuming a dry bulk density of 0.8 [g/cm^3] and a sediment porosity of 0.72. The dry bulk density value is based on a previous study with multicores from the area (Schmidt et al., 2010) and is assumed not to vary substantially over the depth of the core (~15 m).

3.3. Biomarker analyses

Sediment core MD03-2607 was sampled at 5 cm intervals for the first 300 cm and every 10 cm for the rest of the core for biomarker analyses. Sediment samples were freeze-dried, homogenized and extracted using an Automated Solvent Extractor (ASE) 200, DIONEX; 100 °C and 7.6×10^6 Pa with a mixture of dichloromethane (DCM): methanol (MeOH) (9:1, v:v) to obtain a total lipid extract (TLE). Internal standards (squalane, nonadeca-1-one, C_{46} Glycerol Dialkyl Glycerol Tetraether — GDGT) were added to the TLE and subsequently each TLE was separated into an apolar, ketone and polar fraction. The ketone fractions were analyzed by gas chromatography (GC) and gas chromatography/mass spectrometry (GC/MS) and the polar fractions were analyzed by GC/MS.

Table 1
Average water content, supported and unsupported dry dose rate, environmental dose rate, equivalent dose (D_e) and age for OSL samples from selected horizons in core MD03-2607.

Sample depth (cm)	Measured water content (%)	Modeled water content (%)	Supported dry dose rate (mGy/ka)	Unsupported dry dose rate (mGy/ka)	Environmental dose rate (Gy/ka)	Equivalent dose[a] (Gy)	Sample age (ka)
0–1	51	64±5	58.8±12	4.1±0.3	0.34±0.03	0.39±0.04	1.07±0.16
24.5–25.5	52	60±5	63.5±12	4.7±0.3	0.37±0.03	0.91±0.13	2.38±0.41
32.5–33.5	51	58±5	66.4±16	5.5±0.3	0.40±0.03	1.25±0.24	3.11±0.67
49.5–50.5	49	59±5	74.0±17	6.3±0.4	0.44±0.04	1.74±0.22	3.94±0.61
63.5–64.5[b]	48	56±5	76.1±15	9.1±0.5	0.46±0.04	14.92±0.35	24.06±2.16
74.5–75.5	47	54±5	77.3±11	10.0±0.5	0.47±0.04	2.55±0.19	5.37±0.61
99.5–101.5	44	49±5	93.6±27	22.8±1.0	0.60±0.05	5.98±0.81	9.98±1.61
124.5–125.5	45	50±5	109±25	25.8±1.2	0.69±0.06	7.83±0.43	11.35±1.11
149.5–150.5	49	54±5	124±29	34.3±1.5	0.76±0.06	11.86±0.34	15.52±1.30
174.5–175.5[c]	72	75±5	197±43	44.3±1.9	1.05±0.08	13.39±1.72	12.75±1.89
199.5–200.5	75	79±5	272±31	44.6±1.9	1.40±0.09	24.75±0.94	17.60±1.36
239.5–240.5	74	76±5	291±31	53.0±2.3	1.54±0.10	30.51±0.79	19.72±1.39
279.5–280.5	62	66±5	271±28	58.1±2.5	1.53±0.10	29.98±3.19	19.58±2.48

[a] The D_e error term incorporates curve fitting errors and an additional 2.5% systematic measurement error.
[b] Suspected turbidite.
[c] Confirmed turbidite (Wilkins, 2009).

Table 2
Calibrated radiocarbon results from core MD03-2607 and multi-core MC03.

Sample depth and dated material	Sample Code	pMC[a]	$\delta^{13}C$ ‰[b]	Conventional age (^{14}C yr BP)	Calibrated date[c] (ΔR 461 ± 29)[e] (ΔR 1060 ± 70)[d]
MC-03 0.5 cm *Globigerina bulloides*	OZH 736	83.37 ± 0.71	−1.2 ± 0.2	1460 ± 705	(Modern)[d]
0.5 cm planktonic[f]	ANUA 29624	73.10 ± 1.73	−0.5 ± 0.2	2600 ± 190	1090 ± 200[d]
25 cm *G. bulloides*	ANUA 29003	61.38 ± 1.37	0.0 ± 0.2	4010 ± 180	2690 ± 250[d]
40 cm planktonic	ANUA 29625	61.12 ± 1.42	0.2 ± 0.2	4045 ± 185	2740 ± 260[d]
50 cm planktonic	ANUA 29004	53.19 ± 1.20	−0.5 ± 0.2	5155 ± 180	4140 ± 260[d]
75 cm planktonic	ANUA 29626	41.48 ± 1.01	−0.1 ± 0.2	7155 ± 195	6530 ± 230[d]
85 cm planktonic	ANUA 29627	39.23 ± 0.96	−0.3 ± 0.2	7600 ± 195	7040 ± 230[d]
95 cm planktonic	ANUA 29630	30.13 ± 0.83	−0.3 ± 0.2	9720 ± 220	9280 ± 280[d]
100 cm planktonic	ANUA 29631	28.41 ± 0.76	−0.4 ± 0.2	10,190 ± 215	9880 ± 280[d]
140 cm planktonic	ANUA 31203	20.71 ± 0.53	−1.1 ± 0.2	12,730 ± 205	14,260 ± 345[e]
150 cm planktonic	ANUA 29005	18.53 ± 0.51	−0.7 ± 0.2	13,620 ± 220	15,560 ± 335[e]
165 cm planktonic	ANUA 29628	15.54 ± 0.45	−0.7 ± 0.2	15,040 ± 235	17,570 ± 425[e]
175 cm planktonic	ANUA 29006	12.47 ± 0.38	0.0 ± 0.2	16,810 ± 240	19,550 ± 255[e]
175 cm planktonic	ANUA 30504	10.44 ± 0.30	0.0 ± 0.2	18,240 ± 230	20,470 ± 265[e]
175 cm benthic	ANUA 30503	11.02 ± 0.29	0.0 ± 0.2	17,800 ± 210	20,980 ± 345[e]
200 cm planktonic	ANUA 29007	14.07 ± 0.40	0.3 ± 0.2	15,840 ± 225	18,730 ± 210[e]
240 cm planktonic	ANUA 29008	11.43 ± 0.34	0.4 ± 0.2	17,510 ± 240	20,030 ± 115[e]
260 cm planktonic	ANUA 29629	10.74 ± 0.33	−0.4 ± 0.2	18,010 ± 245	20,710 ± 320[e]
280 cm planktonic	ANUA 29009	9.95 ± 0.32	0.0 ± 0.2	18,630 ± 260	21,630 ± 390[e]
300 cm planktonic	ANUA 31204	9.34 ± 0.25	0.4 ± 0.2	19,130 ± 215	22,240 ± 225[e]
360 cm planktonic	ANUA 31205	7.02 ± 0.33	0.2 ± 0.2	21,420 ± 380	25,140 ± 490[e]
430 cm planktonic	ANUA 29010	2.17 ± 0.14	0.0 ± 0.2	30,850 ± 500	35,910 ± 500[e]

[a] Percent modern carbon (pMC) has been corrected for machine background and carbonate preparation background.
[b] $\delta^{13}C$ corrections are from material measured by Gingele et al. (2004).
[c] All radiocarbon ages were calibrated in Calib 5.0.1 (Stuiver and Reimer, 1993), assuming a sample age-span of 100 yr, and applying the Marine04 dataset of Hughen et al. (2004) for ages <26.0 ka, and the polynomial of Bard (1998) for ages >26.0 ka.
[d] Dates corrected with the core-top reservoir age from MC03 (equivalent to a ΔR of 1060 ± 70 yr) prior to calibration.
[e] A regionally corrected marine reservoir of 461 ± 29 yr has been subtracted from the corrected radiocarbon age prior to calibration.
[f] Planktonic samples consisted primarily of *G. bulloides* supplemented with *Globigerinoides ruber*. The benthic sample was composed of *Cibicidoides mundulus* and *Cibicidoides wuellerstorfi*.

3.3.1. Gas chromatography analyses

The ketone fractions were analyzed by a Hewlett Packard 6890 GC, fitted with a 50 m, silica column with 0.32 mm of diameter and coated with CP Sil-5 (thickness = 0.12 μm). The carrier gas was helium. The oven was programmed from 70 °C at injection, then increased by 20 °C min^{-1} to 200 °C and next by 3 °C min^{-1} until 320 °C. The final temperature of 320 °C was held for 30 min. Concentrations of alkenones were calculated using nonadeca-1 — one as internal standard. $U^{K'}_{37}$ was calculated using the equation described by Prahl and Wakeham (1987) and SST values were estimated using the calibration of Müller et al. (1998) as this is the most commonly used global core top calibration, including in our study site (Calvo et al., 2007). Mass accumulation rates of the alkenones were estimated as described for TOC.

3.3.2. Gas chromatography/mass spectrometry analyses

Compound identification of alkenones and long chain diols was conducted using a Thermo Finnigan Trace Ultra GC connected to Thermofinnigan DSQ MS operated at 70 eV, with a mass range m/z 50–800 and 3 scans s^{-1}. The column is a 25 m, silica column with 0.32 mm of diameter and coated with CP Sil-5 (thickness = 0.12 μm). The temperature program initiated at 70 °C, increased first at a rate of 20 °C min^{-1} to 130 °C, and next at a rate of 4 °C min^{-1} to the final temperature of 320 °C, which was held for 10 min. The relative abundances of diols were measured using the same GC/MS operated in single ion mode, monitoring ions of m/z 299, 313 and 327, with a dwell time of 100 ms and ionization energy of 70 eV. The Diol index was calculated using the equation described by Rampen et al. (2008):

$$\text{Diol index} = \frac{[C_{28} + C_{30}\,1,14\text{−diol}]}{[C_{28} + C_{30}\,1,14\text{−diol}] + [C_{30}\,1,15\text{−diol}]}.$$

4. Results and discussion

4.1. Age model of core MD03-2607 and sedimentation rates

The thirteen OSL dates are shown in Table 1. Excluding a suspected poorly bleached sample at 63 cm, the 5 OSL dates from the top 75 cm of the core are consistent with a linear sedimentation rate of 0.17 mm yr^{-1}, implying the loss of approximately 19 cm of sediment from the top of the profile during coring. The three dates between 100 and 150 cm indicate a slower rate of deposition during the early Holocene and the end of MIS 2 (average of 0.07 mm yr^{-1}). The period immediately following the Last Glacial Maximum (LGM), dates between 20 and 15 ka, is characterized by the most rapid sediment deposition (up to 0.29 mm yr^{-1}). Planktonic foraminifera specimens used for ^{14}C dating consist of either monospecific *G. bulloides* or mixed *G. bulloides* and *G. ruber*, and are thus representative of the Flinders Undercurrent or a mixed surface/intermediate water age (Moros et al., 2009). Comparison of the ^{14}C dates with OSL dating shows that during the mid to late Holocene, the OSL dates consistently underestimate the ^{14}C dates adjusted with the published regional reservoir correction, with an average discrepancy of 1250 ± 340 years (Wilkins, 2009). The age offset is within statistical uncertainty of the reservoir age calculated from the core-top sample from multi-core MC03 (1460 ± 70 ^{14}C yr BP). We therefore used a reservoir age correction of 1460 ± 70 years rather than the published regional marine reservoir of 461 ± 29 years (Reimer and Reimer, 2001) to obtain consistent AMS ^{14}C and OSL dates for the Holocene. During the LGM and the deglaciation, the ^{14}C dates were corrected with the published regional marine reservoir of 461 ± 29 years.

The $\delta^{18}O$ record of *G. bulloides* clearly shows similar variations to those of the stacked benthic foraminifera record (Lisiecki and Raymo, 2005), spanning from MIS 1 to the latest part of MIS 6 (Fig. 2). Our

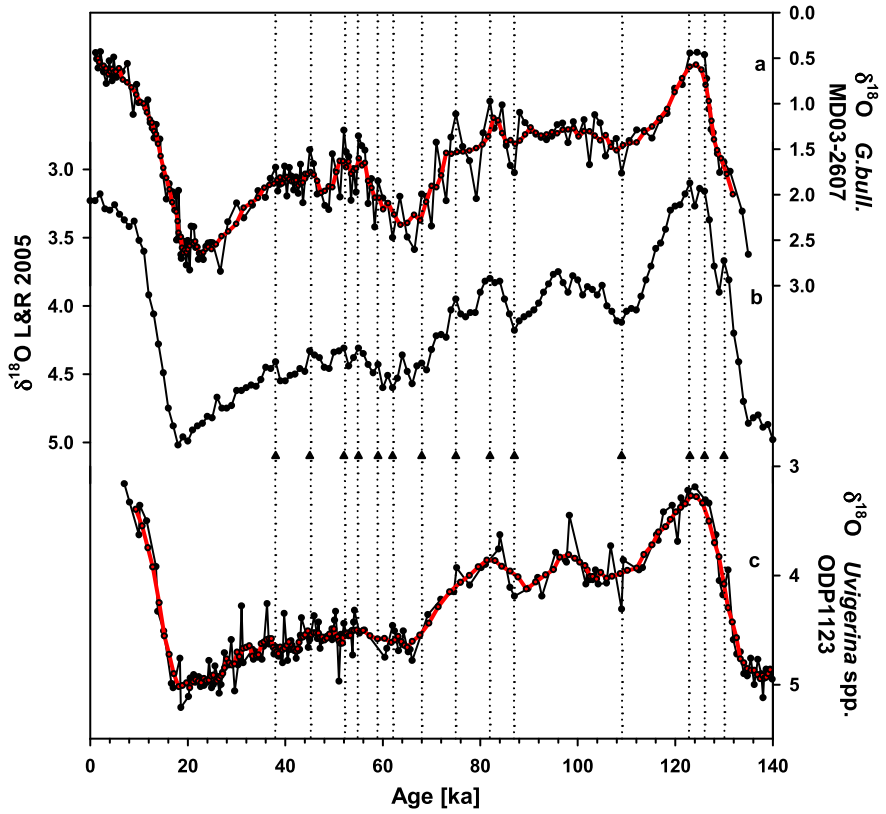

Fig. 2. Comparison of the age model stratigraphy of core MD03-2607. (a) $\delta^{18}O$ of *Globigerina bulloides* of core MD03-2607 located offshore Southeastern Australia. (b) Global stack of benthic foraminifera (Lisiecki and Raymo, 2005). (c) $\delta^{18}O$ of benthic foraminifera *Uvigerina* spp. from core ODP1123 (Elderfield et al., 2010), east of New Zealand. The red line represents smoothed line of 5 points mean; triangles and dotted vertical lines represent tie points used to tune $\delta^{18}O$ record of core MD03-2607 to that of Lisiecki and Raymo (2005).

revised age model for MD03-2607 also compares well with the age model of Gingele and De Deckker (2005). The good correspondence of the $\delta^{18}O$ record of the planktonic foraminifera *G. bulloides* with the stacked benthic foraminiferal isotope records and the consistent AMS ^{14}C and OSL dates confirm that resedimentation caused by turbidic layers (see Table 1) was possibly not a major issue for this core (cf. Gingele and De Deckker, 2005).

Sedimentation rates of sediments from the deeper part of the core were in general 0.1 mm yr^{-1} with peaks during interglacials and MIS 3 of up to 0.2 mm yr^{-1}. The highest peak in the sedimentation rate was during LGM, where values of 0.3–0.8 mm yr^{-1} were recorded (Fig. 3h). The higher sediment rates during the LGM are probably due to the sea level lowstand at that time, through which the Murray River mouth was closer to the site (see Gingele and De Deckker, 2005). Our calculated sedimentation rates compare well with those of Gingele and De Deckker (2005), although our higher resolution record now yields more detailed sedimentation rate changes.

4.2. Carbon isotope record of foraminifera

The $\delta^{13}C$ record of *G. bulloides* shows distinct sharp minima associated with the deglaciation periods antecedent to MIS 5e and 1, and the MIS4/3 transition (yellow bars, Fig. 3c). Minima in stable carbon isotopic values of planktonic foraminifera can in principle be caused for a variety of reasons. For instance, the input of terrestrial organic matter and subsequent oxidation can lower the $\delta^{13}C$ of dissolved inorganic carbon. However, the $\delta^{13}C$ of the sedimentary organic carbon was relatively constant at −22 to −23‰ (Lopes dos Santos et al., unpublished data) suggesting that the input of terrestrial organic matter did not substantially change over time. A lower primary productivity and low nutrient concentrations can lead to a decrease in CO_2 uptake, leading to a decrease in $\delta^{13}C$ of dissolved inorganic carbon and thus to a decrease in the planktonic $\delta^{13}C$ record. However, as will be discussed below, the productivity records do not match the planktonic foraminifera record. Thus, we suggest that these minima probably represent an isotopic signal of SO waters which contain ^{13}C-depleted CO_2 (Spero and Lea, 2002; Pena et al., 2008; Calvo et al., 2011; Hayes et al., 2011). Indeed, the timing and distribution of the deglacial carbon isotope are consistent with those of other planktonic foraminifera records used elsewhere to infer the influx of SO waters (Spero and Lea, 2002; Pena et al., 2008; Calvo et al., 2011; Hayes et al., 2011). This suggests that the Murray Canyons Group area received an influx of SO waters, during the deglaciations and the MIS4/3 transition. Gingele and De Deckker (2005) also reported minima in their $\delta^{13}C$ record of *G. bulloides* but, due to the lower resolution of their record, the first two isotopic minima were not apparent in their record. These minima in planktonic $\delta^{13}C$ record is not directly interpreted as upwelling *per se* in this study since it has evidence based on barium concentrations that deeper waters can be brought up in the canyons, but not up to the surface.

4.3. Sea-surface temperature record

We generated a sea-surface temperature (SST) record based on the $U^{K'}_{37}$ of the alkenones (Prahl and Wakeham, 1987; Müller et al., 1998). The uppermost core sample shows a temperature of 18 °C in agreement with the modern SST range in this area (14–18 °C) (Locarnini et al., 2010). The $U^{K'}_{37}$ SST record shows a good correspondence with our $\delta^{18}O$ record of *G. bulloides* (Fig. 3a, b), displaying the warmest temperature of ~21 °C during the last interglacial (MIS 5e), slightly warmer than the present interglacial with ~20 °C (MIS 1). The lowest temperature was recorded during the LGM with a temperature of

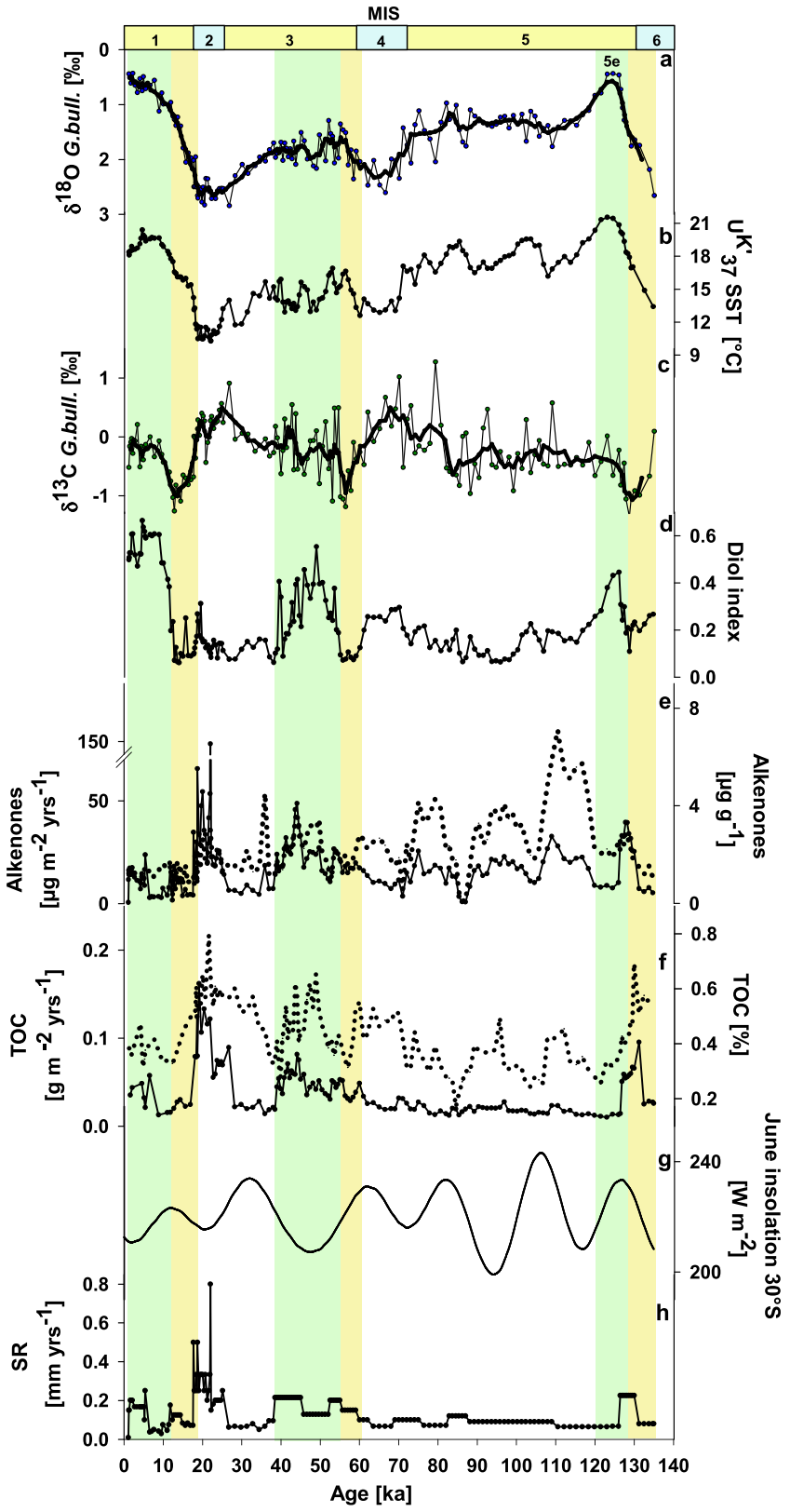

Fig. 3. Geochemical records from core MD03-2607. (a) $\delta^{18}O$ of *Globigerina bulloides*. Thick line represents the smoothed 5 points mean. (b) $U^{K'}_{37}$ SST. (c) $\delta^{13}C$ of *G. bulloides*. Thick line represents the smoothed 5 points mean. (d) Diol index. (e) Alkenone concentration (dotted line) and accumulation rates (plain line). (f) Total Organic Carbon (TOC) percentage (dotted line) and accumulation rates (plain line). (g) June insolation at 30°S. (h) Sedimentation Rate (SR). MIS stands for Marine Isotope Stages. Yellow shaded bars are periods of minima in planktonic $\delta^{13}C$ suggesting influence of Southern Ocean waters and green shaded bars are peak periods in diol index suggesting blooms in *Proboscia* diatoms.

~10 °C. The last deglaciation was characterized by a warming of ~10 °C with a clear interruption from 16 to 13 ka, comparable with the interruption reported in the $U^{K'}_{37}$ SST record of the nearby core MD03-2611, which is ca. 80 km south-east of our core (Calvo et al., 2007).

4.4. Productivity in the Murray Canyons area

Several proxies were used to reconstruct a high-resolution productivity record offshore Southeastern Australia. We first generated a high-resolution record of % TOC and TOC accumulation rates (TOC AR) as an indicator for general productivity as well as biomarker records for specific algae, i.e. alkenone concentrations and accumulation rates (alkenone AR) and the Diol index. The potential controls on the productivity records are subsequently discussed.

4.4.1. General productivity

TOC varied from 0.2 to 0.8% with maxima during the LGM and minima at 85 ka. The TOC AR shows a relatively similar pattern as % TOC suggesting that the TOC record is not strongly affected by dilution of inorganic material. The TOC AR had maximum values of 0.2 and 0.1 g m^{-2} yr^{-1} at the LGM and the penultimate deglaciation, followed by lower peaks during MIS 1 and 3 (Fig. 3f). This is similar to the findings of Gingele and De Deckker (2005), who found higher TOC contents during the LGM and the penultimate deglaciation. This increase of TOC AR could in principle be caused by increased terrigenous carbon input from the Murray–Darling River as the sea level stand was lower and the core site was then closer to the river mouth (Gingele et al., 2004). However, Gingele and De Deckker (2005) did not find elevated C/N ratios during these times, suggesting no increased input of terrestrial organic matter. Additionally, $\delta^{13}C$ values of sedimentary organic matter during glacials were rather constant at −22 to −23‰ (Lopes dos Santos et al., unpublished data), values corresponding to those of marine organic matter (Meyers, 1994) and suggesting no substantial increase in the delivery of terrestrial OC. Based on this, we assume that the TOC reflects mainly marine OC.

A comparison of the TOC records with the planktonic foraminiferal carbon isotope record shows that most maxima in TOC do not match with minima in $\delta^{13}C$, suggesting that an influx of deep SO waters did not have a large influence on general productivity. Gingele and De Deckker (2005) inferred that the increased TOC during glacials may be due to stronger winds as they found a correlation between their TOC record and June insolation minima at 30°S. Indeed, we also find a reasonable match between maxima in our high-resolution TOC record and insolation minima (Fig. 3f, g), suggesting that stronger winds could play a role in the increased productivity. During insolation minima, the anticyclonic center lies over central Australia and the westerlies occur over this region (Sturman and Tapper, 1996). The stronger winds have the potential to bring aeolian dust to our core site (Gingele and De Deckker, 2005; Gingele et al., 2007), thereby fertilizing the surface waters, as well as enhancing the mixing of waters from below the surface thereby providing an influx of deeper nutrient-rich waters, as postulated by Passlow et al. (1997) for core E55-6 offshore Victoria. Unfortunately, the *n*-alkane's record at this site seems to be more related to fluvial input as it correlates with the BIT index (Hopmans et al., 2004), a proxy for soil input organic matter mainly transported by rivers. Thus, further studies, reconstructing e.g. aeolian input, are needed to provide evidence for this hypothesis.

4.4.2. Haptophyte productivity

Alkenone concentrations ranged from 0.1 to 7 μg g^{-1} with the lowest values at 86 ka and highest values at 110 ka (Fig. 3e). The alkenone AR shows a similar pattern as the alkenone concentration although the maximum during LGM is much more dominant due to the larger SR at this time. In principle, biomarker concentrations can be substantially affected not only by production but also by the degree of preservation. For example, an increase in the SR can decrease the time that the biomarkers are exposed to the oxygen, leading to an increased preservation and concentration. However, as the highest concentrations are observed during periods of low SR, we assume that the alkenones are not substantially affected by preservation. In agreement with the TOC, the maxima in alkenone concentration and AR do not match minima in the foraminiferal carbon isotope record, suggesting that influx of deep SO waters apparently did not stimulate haptophyte algal productivity to any great extent. In contrast, the increased haptophyte productivity is mainly during insolation minima, possibly due to stronger offshore winds such as the westerlies, as well as winds from inland Australia that may have increased the input of nutrients to this site.

4.4.3. Proboscia diatom productivity

Finally, we investigated the sediments for potential biomarkers of diatoms. Only 1,14-diols, derived from *Proboscia* diatoms (Sinninghe Damsté et al., 2003), were present in relatively high amounts, while other potential diatom biomarkers, such as highly branched isoprenoids (Volkman et al., 1994), were not detected and only low amounts of the somewhat more ambiguous diatom biomarker loliolide (Klok et al., 1984) were detected. We therefore used the Diol index, based on the relative abundance of 1,14-diol versus 1,15-diols, which has been shown to be a suitable recorder of the relative abundance of *Proboscia* diatoms (Rampen et al., 2008). The Diol index clearly shows maxima during MIS 1, 3 and 5e and minimum values during deglaciation periods (Fig. 3d). In contrast to the other productivity records, there is no apparent correlation of the Diol index with insolation minima and, in fact, *Proboscia* diatom productivity was relatively greater during the warm periods.

Comparison with the foraminiferal carbon isotope record shows that peaks in the Diol index lag the start of each of the $\delta^{13}C$ minima by about 10 ka, suggesting that *Proboscia* productivity increased only after the influx of ^{13}C-depleted SO waters diminished. Interestingly, our *Proboscia* diatom productivity matches some diatom productivity records from the Eastern Equatorial Pacific: indeed, higher opal flux burial rates during the Holocene as seen in core V21-40 (Bradtmiller et al., 2006) (Fig. 4c) and during MIS 3 in core TR163-19 (Kienast et al., 2006), both located in the Eastern Equatorial Pacific, display an excellent match with our diol record (Fig. 4b and d). These similar trends suggest that possibly these areas, as well as the Murray Canyons area, simultaneously received input of nutrients, particularly silicic acid, during interglacials which stimulated diatom productivity. A possible scenario which can explain the seemingly contemporaneous elevated diatom productivity in the Equatorial Pacific and *Proboscia* diatom productivity in Southeastern Australia is the transport of nutrients as silicic acid from SO waters. However, if this was the case, then we would expect a match between the maxima in our Diol index record and carbon isotope minima in planktonic foraminifera, a phenomenon that we do not observe. This potentially suggests that the SO waters which reached Southeastern Australia during deglaciations did not contain sufficient nutrients to stimulate productivity offshore Southeastern Australia.

It should be noted that *Proboscia* diatoms are able to build thin frustules and thus can thrive at relatively low concentration of silicic acid (Goering and Iverson, 1981). Indeed, their frustules may be more prone to dissolution in comparison to those of other diatoms (Koning et al., 2001), thus providing an explanation why no diatom frustules were found at this site. Consequently, the amount of silicic acid in the SO waters that reached Southeastern Australia during interglacials and MIS 3 was probably relatively low, but nevertheless sufficient enough to support an increased *Proboscia* diatom productivity, but possibly not of other diatom groups. This suggests that silicic acid, presumably derived from the SO, was predominantly transported to the equatorial Pacific and only to a minor extent to offshore Southeastern

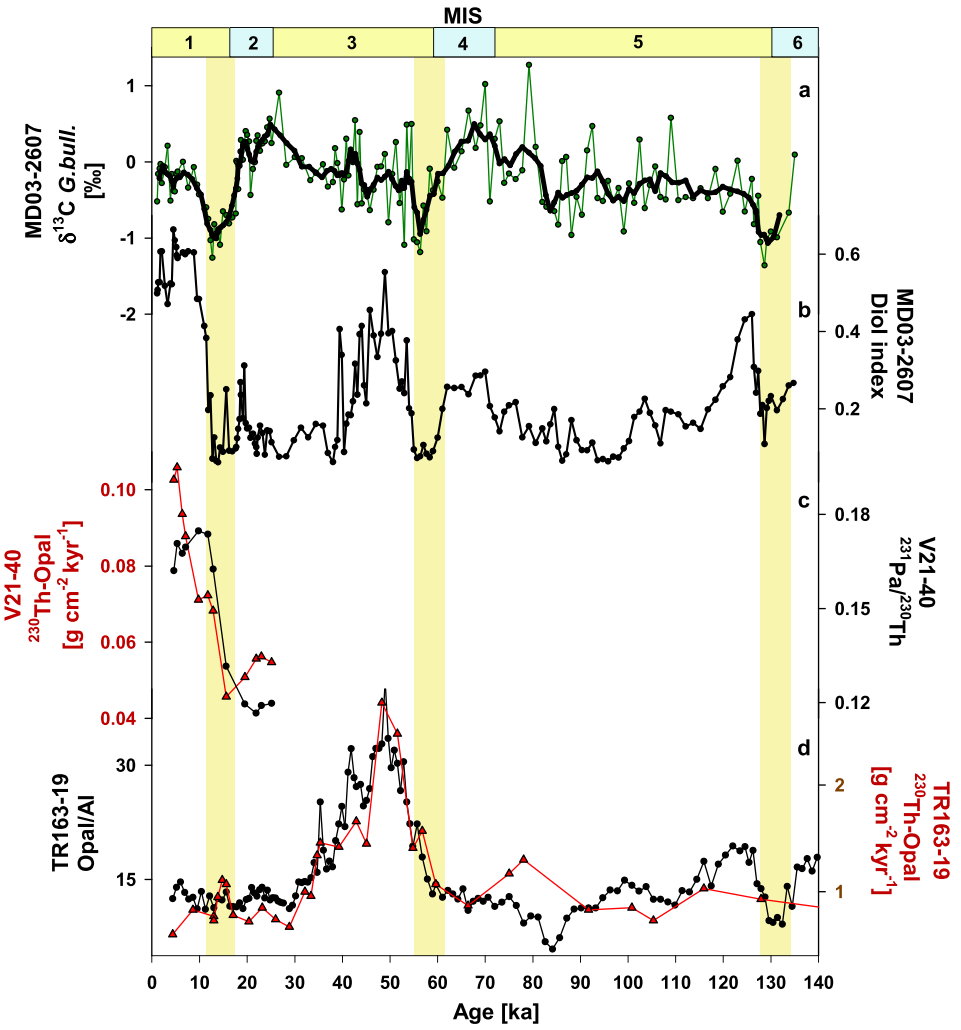

Fig. 4. Geochemical records from offshore Southeastern Australia and from selected cores from different latitudes. (a) $\delta^{13}C$ of *G. bulloides* from core MD03-2607. (b) Diol index record from core MD03-2607. (c) $^{231}Pa/^{230}Th$ in black and ^{230}Th-normalized opal flux in red from core V21-40 in East Equatorial Pacific (Bradtmiller et al., 2006). (d) Biogenic opal/aluminum ratios in black and ^{230}Th-normalized opal flux in red of core TR163-19 in the Eastern Equatorial Pacific (Kienast et al., 2006). MIS (Marine Isotope Stages). Yellow shaded bars represent periods of minima in planktonic $\delta^{13}C$.

Australia during these periods. This could possibly explain the apparent enigma that *Proboscia* diatom productivity was stimulated while no minima in $\delta^{13}C$ planktonic foraminifera record were apparent.

5. Conclusions

High resolution records of past productivity offshore Southeastern Australia show strong variations for the last ~135 ka. The highest primary productivity is observed during the LGM and is, possibly, linked to the stronger winds (e.g. the westerlies), causing an increased dust supply from inland Australia to the core site, as well as mixing of the water column that would have brought nutrient-rich waters to the surface. Diatom productivity at the Murray Canyons Group area seems to be limited, as the only specific biomarkers for diatoms found were long chain 1,14 diols and no silica frustules were found in the sediments. The reconstructed *Proboscia* diatom productivity, based on the Diol index, was higher during interglacials and MIS 3, concomitant with diatom productivity increases in the equatorial Pacific, but not with minima in the planktonic foraminiferal record, an indicator for SO water influx. This can tentatively be explained by a minor input of silicic acid transport from the SO as *Proboscia* diatoms only require low amounts of silica. Further studies on past changes in ocean currents are needed for a better understanding of the mechanism which transports nutrients from the SO to lower latitudes.

Acknowledgments

We thank Sebastiaan Rampen, Anchelique Mets and Judith Shelley for analytical assistance. Mrs Judith Shelley prepared some of the additional planktonic foraminifers that were analyzed at NIOZ. Research funding was provided by a VICI grant to SS from the Netherlands Organization of Scientific Research. Core MD03-2607 was obtained with a National Oceans Office grant and an Australian Research Council grant, both awarded to PDD. Y. Balut from IPEV was instrumental in obtaining the core. DW acknowledges help from J. Olley [CSIRO Canberra] and L.K. Fifield [ANU] with dating procedures and provision of facilities. Dating by DW was funded by ARC grant (DP034493) and AINSE grant (AINGRA07037).

References

Bard, E., 1998. Geochemical and geophysical implications of the radiocarbon calibration. Geochimica et Cosmochimica Acta 62 (12), 2025–2038.

Bradtmiller, L.I., Anderson, R.F., Fleisher, M.Q., Burckle, L.H., 2006. Diatom productivity in the equatorial Pacific Ocean from the last glacial period to the present: a test of the silicic acid leakage hypothesis. Paleoceanography 21 (4) (PA4201-1-PA4201-12).

Brzezinski, M.A., Pride, C.J., Franck, V.M., Sigman, D.M., Sarmiento, J.L., Matsumoto, K., Gruber, N., Rau, G.H., Coale, K.H., 2002. A switch from $Si(OH)_4$ to NO^{-3} depletion in the glacial Southern Ocean. Geophysical Research Letters 29 (12) (1564-1564-4).

Calvo, E., Pelejero, C., De Deckker, P., Logan, G.A., 2007. Antarctic deglacial pattern in a 30 kyr record of sea surface temperature offshore South Australia. Geophysical Research Letters 34 (13) (L13707-1-L13707-6).

Calvo, E., Pelejero, C., Pena, L.D., Cacho, I., Logan, G.A., 2011. Eastern equatorial Pacific productivity and related-CO_2 changes since the last glacial period. Proceedings of the National Academy of Sciences Early Edition 1–5.

Crosta, X., Beucher, C., Pahnke, K., Brzezinski, M.A., 2007. Silicic acid leakage from the Southern Ocean: opposing effects of nutrient uptake and oceanic circulation. Geophysical Research Letters 34 (13). http://dx.doi.org/10.1029/2006GL029083 (L13601-1-L13601-5).

De Deckker, P., Moros, M., Perner, K., Jansen, E., 2012. Influence of the tropics and de southern westerlies on glacial interhemispheric asymmetry. Nature Geoscience 5, 266–269.

Elderfield, H., Greaves, M., Barker, S., Hall, I.R., Tripati, A., Ferretti, P., Crowhurst, S., Booth, L., Daunt, C., 2010. A record of bottom water temperature and seawater delta O-18 for the Southern Ocean over the past 440 kyr based on Mg/Ca of benthic foraminiferal *Uvigerina* spp. Quaternary Science Reviews 29 (1–2), 160–169.

Fifield, L.K., Allan, G.L., Stone, J.O.H., Ophel, T.R., 1994. The ANU AMS system and research program. Nuclear Instruments and Methods 92 (1–4), 85–88.

Fink, D., Hotchkis, M., Hua, Q., Jacobsen, G., Smith, A.M., Zoppi, U., Child, D., Mifsud, C., van der Gaast, H., Williams, A., Williams, M., 2004. The ANTARES AMS facility at ANSTO. Nuclear Instruments and Methods in Physics Research Section B: Beam Interactions with Materials and Atoms 223–224, 109–115.

Gingele, F.X., De Deckker, P., 2005. Late Quaternary fluctuations of palaeoproductivity in the Murray canyons area, South Australian continental margin. Palaeogeography, Palaeoclimatology, Palaeoecology 220 (3–4), 361–373.

Gingele, F.X., De Deckker, P., Hillenbrand, C.-D., 2004. Late Quaternary terrigenous sediments from the Murray Canyons area, offshore South Australia and their implications for sea level change, palaeoclimate and palaeodrainage of the Murray–Darling Basin. Marine Geology 212 (1–4), 183–197.

Gingele, F., De Deckker, P., Norman, M., 2007. Late Pleistocene and Holocene climate of SE Australia reconstructed from dust and river loads deposited offshore the River Murray Mouth. Earth and Planetary Science Letters 255 (3–4), 257–272.

Goering, J.J., Iverson, R.I., 1981. Phytoplankton distribution on the southeastern Bering Sea shelf. In: Hood, D.J., Calder, J.A. (Eds.), The Eastern Bering Sea Shelf: Oceanography and Resources, 2. University of Washington Press, Seattle, pp. 933–946.

Hayes, C.T., Anderson, R.F., Fleisher, M.Q., 2011. Opal accumulation rates in the equatorial Pacific and mechanisms of deglaciation. Paleoceanography 26, PA1207. http://dx.doi.org/10.1029/2010PA002008.

Hill, P.J., De Deckker, P., 2004. AUSCAN seafloor mapping and geological sampling survey on the Australian southern margin by RV *Marion Dufresne* in 2003: final project report. Geoscience Australia Record 2004/4 (Petroleum and Marine Division), pp. 1–144.

Hopmans, E.C., Weijers, J.W.H., Schefuß, E., Herfort, L., Sinninghe Damsté, J.S., Schouten, S., 2004. A novel proxy for terrestrial organic matter in sediments based on branched and isoprenoid tetraether lipids. Earth and Planetary Science Letters 224 (1–2), 107–116.

Horn, M.G., Beucher, C.P., Robinson, R.S., Brzezinski, M.A., 2011. Southern ocean nitrogen and silicon dynamics during the last deglaciation. Earth and Planetary Science Letters 310, 334–339.

Hughen, K.A., Baillie, M.G.L., Bard, E., Beck, J.W., Bertrand, C.J.H., Blackwell, P.G., Buck, C.E., Burr, G.S., Cutler, K.B., Damon, P.E., Edwards, R.L., Fairbanks, R.G., Friedrich, M., Guilderson, T.P., Kromer, B., McCormac, G., Manning, S., Ramsey, C.B., Reimer, P.J., Reimer, R.W., Remmele, S., Southon, J.R., Stuiver, M., Talamo, S., Taylor, F.W., van der Plicht, J., Weyhenmeyer, C.E., 2004. Marine04 marine radiocarbon age calibration, 026 Cal Kyr BP. Radiocarbon 46, 1059–1086.

Kienast, S.S., Kienast, M., Jaccard, S., Calvert, S.E., Francois, R., 2006. Testing the silica leakage hypothesis with sedimentary opal records from the eastern equatorial Pacific over the last 150 kyrs. Geophysical Research Letters 33 (15) (L15607-1-L15607-4).

Klok, J., Baas, M., Cox, H.C., de Leeuw, J.W., Schenck, P.A., 1984. Loliolides and dihydroactinidiolide in a Recent marine sediment probably indicate a major transformation pathway of carotenoids. Tetrahedron Letters 25 (48), 5577–5580.

Koning, E., van Iperen, J.M., van Raaphorst, W., Helder, W., Brummer, G.-J.A., van Weering, T.C.E., 2001. Selective preservation of upwelling-indicating diatoms in sediments off Somalia, NW Indian Ocean. Deep-Sea Research I 48, 2473–2495.

Lisiecki, L.E., Raymo, M.E., 2005. A Pliocene–Pleistocene stack of 57 globally distributed benthic $\delta^{18}O$ records. Paleoceanography 20 (1) (PA1003-PA1003-17).

Locarnini, R.A., Mishonov, A.V., Antonov, J.I., Boyer, T.P., Garcia, H.E., Baranova, O.K., Zweng, M.M., Johnson, D.R., 2010. World Ocean Atlas 2009, Volume 1: Temperature. In: Levitus, S. (Ed.), NOAA Atlas NESDIS 68. U.S. Government Printing Office, Washington, D.C.

Matsumoto, K., Sarmiento, J.L., Brzezinski, M.A., 2002. Silicic acid leakage from the Southern Ocean: a possible explanation for glacial atmospheric pCO_2. Global Biogeochemical Cycles 16 (3), 1–23. http://dx.doi.org/10.1029/2001GB001442.

Meyers, P.A., 1994. Preservation of elemental and isotopic source identification of sedimentary organic-matter. Chemical Geology 114 (3–4), 289–302.

Middleton, J.F., Bye, J.A.T., 2007. A review of the shelf-slope circulation along Australia's southern shelves: Cape Leeuwin to Portland. Progress in Oceanography 75 (1), 1–41.

Moros, M., De Deckker, P., Jansen, E., Perner, K., Telford, R.J., 2009. Holocene climate variability in the Southern Ocean recorded in a deep-sea sediment core off South Australia. Quaternary Science Reviews 28 (19–20), 1932–1940.

Müller, P.J., Kirst, G., Ruhland, G., von Storch, I., Rosell-Mele, A., 1998. Calibration of the alkenone paleotemperature index ($U^{K'}_{37}$) based on core-tops from the eastern South Atlantic and the global ocean (60°N–60°S). Geochimica et Cosmochimica Acta 62 (10), 1757–1772.

Olley, J.M., Pietsch, T., Roberts, R.G., 2004. Optical dating of Holocene sediments from a variety of geomorphic settings using single grains of quartz. Geomorphology 60 (3–4), 337–358.

Passlow, V., Wang, P., Chivas, A.R., 1997. Late Quaternary palaeoceanography near Tasmania, southern Australia. Palaeogeography, Palaeoclimatology, Palaeoecology 131 (3–4), 433–463.

Pena, L.D., Cacho, I., Ferretti, P., Hall, M.A., 2008. El Niño–Southern Oscillation-like variability during glacial terminations and interlatitudinal teleconnections. Paleoceanography 23 (3), PA3101-8.

Prahl, F.G., Wakeham, S.G., 1987. Calibration of unsaturation patterns in long-chain ketone compositions for palaeotemperature assessment. Nature 330, 367–369.

Rampen, S.W., Schouten, S., Koning, E., Brummer, G.-J.A., Sinninghe Damsté, J.S., 2008. A 90 kyr upwelling record from the northwestern Indian Ocean using a novel long-chain diol index. Earth and Planetary Science Letters 276 (1–2), 207–213.

Reimer, P.J., Reimer, R.W., 2001. A marine reservoir correction database and on-line interface. Radiocarbon 43, 461–463.

Romero, O., Mollenhauer, G., Schneider, R.R., Wefer, G., 2003. Oscillations of the siliceous imprint in the central Benguela Upwelling System from MIS 3 through to the early Holocene: the influence of the Southern Ocean. Journal of Quaternary Science 18 (8), 733–743.

Sarmiento, J.L., Gruber, N., Brzezinski, M.A., Dunne, J.P., 2004. High-latitude controls of thermocline nutrients and low latitude biological productivity. Nature 427 (6969), 56–60.

Schmidt, S., De Deckker, P., Etcheber, H., Caradec, S., 2010. Are the Murray Canyons offshore southern Australia still active for sediment transport? Geological Society of London, Special Publications 346, 43–55. http://dx.doi.org/10.1144/SP346.4.

Sinninghe Damsté, J.S., Rampen, S., Rijpstra, W.I.C., Abbas, B., Muyzer, G., Schouten, S., 2003. A diatomaceous origin for long-chain diols and mid-chain hydroxy methyl alkanoates widely occurring in Quaternary marine sediments: indicators for high-nutrient conditions. Geochimica et Cosmochimica Acta 67 (7), 1339–1348.

Smith, S.L., 2001. Understanding the Arabian Sea: reflections on the 1994–1996 Arabian Sea expedition. Deep-Sea Research II 48, 1385–1402.

Spero, H.J., Lea, D.W., 2002. The cause of carbon isotope minimum events on glacial terminations. Science 296, 522–525.

Stokes, S., Ingram, S., Aitken, M.J., Sirocko, F., Anderson, R., Leuschner, D., 2003. Alternative chronologies for Late Quaternary (Last Interglacial–Holocene) deep sea sediments via optical dating of silt-sized quartz. Quaternary Science Reviews 22 (8–9), 925–941.

Stuiver, M., Reimer, P.J., 1993. Extended ^{14}C database and revised CALIB 3.0 14C age calibration program. Radiocarbon 35 (1), 215–230.

Sturman, S., Tapper, N., 1996. The Weather and Climate of Australia and New Zealand. Oxford University Press, Australia, pp. 1–476.

Toggweiler, J.R., Dixon, K., Broecker, W.S., 1991. The Peru upwelling and the ventilation of the South-Pacific thermocline. Journal of Geophysical Research-Oceans 96 (C11), 20467–20497.

Vogel, J.S., 1984. Performance of catalytically condensed carbon for use in accelerator mass spectrometry. Nuclear Instruments and Methods in Physics Research Section B: Beam Interactions with Materials and Atoms 5 (2), 289–293.

Volkman, J.K., Eglinton, G., Corner, E.D.S., Forsberg, T.E.V., 1980. Long-chain alkenes and alkenones in the marine coccolithophorid *Emiliania huxleyi*. Phytochemistry 19, 2619–2622.

Volkman, J.K., Barrett, S.M., Dunstan, G.A., Jeffrey, S.W., 1992. C_{30}–C_{32} alkyl diols and unsaturated alcohols in microalgae of the class *Eustigmatophyceae*. Organic Geochemistry 18 (1), 131–138.

Volkman, J.K., Barrett, S.M., Dunstan, G.A., 1994. C_{25} and C_{30} highly branched isoprenoid alkenes in laboratory cultures of two marine diatoms. Organic Geochemistry 21 (3–4), 407–413.

Wilkins, D., 2009. Comparative optically stimulated luminescence (OSL) and AMS radiocarbon dating of Holocene lacustrine and marine deposits in southeast and southwestern Australia. PhD thesis, The Australian National University, Canberra. Australia.

Wilkins, D., De Deckker, P., Fifield, L.K., Gouramanis, C., Olley, J., 2012. Comparative optical and radiocarbon dating of laminated Holocene sediments in two maar lakes: Lake Keilambete and Lake Gnotuk, south-western Victoria, Australia. Quaternary Geochronology 9, 3–15.

Willmott, V., Rampen, S.W., Domack, E., Canals, M., Sinninghe Damsté, J.S., Schouten, S., 2010. Holocene changes in *Proboscia* diatom productivity in shelf waters of the north-western Antarctic Peninsula. Antarctic Science 22 (1), 3–10.